SAND2014-17107J

Photoelectrochemical etching of epitaxial InGaN thin films: self-limited kinetics and nanostructuring

Xiaoyin Xiao*, Arthur J. Fischer, Michael E. Coltrin, Ping Lu, Daniel D. Koleske, George T. Wang, Ronen Polsky, Jeffrey Y. Tsao*

Sandia National Laboratories, Albuquerque, New Mexico, 87175, United States

* Corresponding authors.
E-mail addresses: xnxiao@sandia.gov (X.Y. Xiao), jytsao@sandia.gov (J.Y.Tsao).

ABSTRACT. We report here the characteristics of photoelectrochemical (PEC) etching of epitaxial InGaN semiconductor thin films using narrowband lasers with linewidth less than ~1 nm. In the initial stages of PEC etching, when the thin film is flat, characteristic voltammogram shapes are observed. At low photo-excitation rates, voltammograms are S-shaped, indicating the onset of a voltage-independent rate-limiting process associated with electron-hole-pair creation and/or annihilation. At high photo-excitation rates, voltammograms are superlinear in shape, indicating, for the voltage ranges studied here, a voltage-dependent rate-limiting process associated with surface electrochemical oxidation. As PEC etching proceeds, the thin film becomes rough at the nanoscale, and ultimately evolves into an ensemble of nanoparticles. This change in InGaN film volume and morphology leads to a characteristic dependence of PEC etch rate on time: an incubation time, followed by a rise, then a peak, then a slow decay.

Keywords: III-nitrides, wet chemical process, photoelectrochemical etching, bandgap selection, quantum dots

1. Introduction

III-N materials have a combination of properties unique amongst the known semiconductors [1-6]. They have direct bandgaps which span an extremely wide range from the infrared (0.7 eV for InN, corresponding to a free-space wavelength of ~1770 nm) to the deep ultraviolet (5.6 eV for AlN, corresponding to a free-space wavelength of ~220 nm) and thus with the potential for efficient optoelectronics over a wide wavelength range. They have extremely high figures-of-merit for high-speed and high-power electronics. They have very high piezoelectric coefficients of interest for sensing and actuation. Perhaps most importantly, their high bond strengths give them robustness against environments which subject them to harsh chemicals, high mechanical stresses, high temperatures and intense radiation, including in vivo human and biological environments.

This last property of III-N materials, robustness, makes fabrication of complex device architectures in these materials difficult, however. In nearly all other semiconductors, both additive (e.g., epitaxial growth) and subtractive (e.g., etching) processes are used in combination, often in complex sequences, to enable architectures as varied as integrated optoelectronics, vertical-cavity surface emitting lasers, micro-opto-electromechanical systems, and photonic-crystal photovoltaics. In III-N materials, however, subtractive processes have been problematic: no known chemical etchants have the combination of speed and composition selectivity necessary for practical application [7-13].

Recently, photoelectrochemical (PEC) etching has shown promise for such subtractive processing of III-N materials [14-18]. In conjunction with additive epitaxial processes for compositional layering and narrow-band lasers for compositionally selective photo-excitation, novel and otherwise difficult to fabricate III-N-based structures such as optical microcavities and vertical-cavity surface-emitting lasers have been demonstrated. Moreover, in conjunction with quantum-size effects, our laboratory has recently demonstrated controlled fabrication of sub-10-nm nanostructures [19].

En route to improved control of PEC etching of III-N materials, however, an understanding of its kinetics is desirable. In this paper, we present initial empirical studies of these kinetics. Throughout the work we present in this paper, we use narrowband (~ 1 nm linewidth) tunable lasers to provide accurate and controlled energies for photo-excitation, and we use simple thin-film geometries for ease of interpretation. We study the kinetics of laser-induced PEC etching of these

thin InGaN films as a function of laser wavelength and intensity, as a function of film thickness and geometry, and dynamically over the overall InGaN thin film PEC etching life cycle.

2. Experimental

2.1. Film preparation, absorbance, and chemicals

InGaN and GaN thin films were grown on sapphire templates by metal-organic vapor-phase epitaxy (MOVPE). A thick (4-5 micron) GaN buffer layer was first grown on a sapphire substrate at 1050 °C, followed (in some cases) by a 100-nm-thick $In_{0.02}Ga_{0.98}N$ underlayer, followed by a 3-20-nm-thick $In_{0.13}Ga_{0.87}N$ film grown at 770 °C, finally followed (in some cases) by a 10-nm-thick GaN cap grown at 800 °C. Film absorbance was measured in air and referenced to air using Backman coulter DU 800 spectrophotometer.

For the working electrode we used metallic In electrodes applied to the front of the sample by contact with In wire at 280 °C. The Indium wire was ~ 0.5 mm in diameter and purchased from Indium Corporation of America. For the working electrolyte we used a 0.2M H_2SO_4 aqueous solution rather than the more common KOH aqueous solution, which largely eliminated etching in the absence of light. The H_2SO_4 was ACS grade and purchased from Fisher Scientific.

2.2.Laser setup and electrochemical measurements

The second harmonic of a tunable Ti:sapphire laser (400–500 nm wavelength, 2 ps pulse width, 1 nm linewidth, 82 MHz pulse repetition rate, 10 mW) was used for photo-excitation during PEC etching. Light was directed through an optical fiber, then through a quartz window, then through ~ 1.5 cm of electrolyte, resulting in a ~ 2 cm diameter Gaussian spot on the sample. The samples were suspended in the PEC cell, with PEC etching performed using a CH Instruments 660 electrochemical analyzer. As electrodes, we used a Pt counter electrode and an Ag/AgCl reference electrode from Bioanalytical Systems.

2.3. Atomic force microscopy and image analysis

AFM was performed using an Asylum MFP-3D-S system. All images were taken in air in the AC mode at scan rate ~1 Hz. Image and statistical particle size analyses were performed using Gwyddion software.

2.4. Scanning transmission electron microscopy

Samples were prepared for cross-section by focused ion beam (FIB) milling. We used an FEI Titan G2 80-200 STEM with a Cs probe corrector and ChemiSTEM technology (X-FEG and SuperX EDS with four windowless silicon drift detectors), operated at 200 kV. For chemical mapping, energy-dispersive x-ray spectroscopy (EDS) spectral imaging data was acquired in the GaN [100] zone axis with an electron probe of size less than 0.2 nm, convergence angle of 18.4 mrad, and current of ~100 pA. Spectral imaging was acquired as a series of frames, where the same region was scanned multiple times and frame drift-correction was used between frames to build up spectral imaging data. High-angle annular dark-field (HAADF) images were recorded under similar optical conditions with an annular detector with collection range of 60-160 mrad.

3. Results and discussion

3.1. Thin film microstructure and optical absorption

The microstructure of the InGaN film, and of its interface with the underlying GaN, is shown in the STEM in the inset to Figure 1. The InGaN appears brighter than the GaN due to the higher electron mass of In. EDS mapping showed a uniform distribution of In across the thin film, the In content for the sample in Figure 1 to be 13% (i.e., $In_{0.13}Ga_{0.87}N$).

To understand how the degree of photo-excitation changes with laser wavelength and film thickness, optical absorption spectra of the films were measured. Figure 1 shows the absorption spectrum of a typical sample prior to etching: a 20-nm-thick $In_{0.13}Ga_{0.87}N$ epitaxial film on a 5-µm-thick GaN buffer layer, all on a sapphire substrate. The optical absorption observed at wavelengths below 380 nm is due to the thick GaN underlayer; the optical absorption observed at wavelengths between 380 and 450 nm is due to the thin $In_{0.13}Ga_{0.87}N$ film. The offset of the absorbance is largely due to the light reflection from the film. As In concentration increases, the absorption edge red shifts, corresponding to smaller bandgaps.

The photo-excitation wavelengths of the lasers used in the PEC etching experiments discussed in this paper are indicated by the arrows. The absorption coefficient α of the $In_{0.13}Ga_{0.87}N$ film at these wavelengths can be deduced from the measured absorption A from Figure 1 by the Beer's Law formula $\alpha = -(1/h)\ln(1-A)$, where $h = 20$ nm.

3.2. Dark versus photo-induced electrochemistry

To understand the range of potentials over which no dark electrochemical reaction occurs, the inset to Figure 2 shows a cyclic voltammogram in the initial stages of PEC etching of the InGaN thin film, in the absence of photo-excitation. It can be seen that there is only a non-Faradaic double layer charge-discharge current in the range ~ -0.2-1.6 V. The onset of a Faradaic current at ~ 1.6 V we attribute to oxidation of water. The onset of a Faradaic current at ~ -0.2 V we attribute to hydrogen evolution. Thus, the range of potentials over which no dark electrochemistry occurs is relatively large, and in the following we are careful to stay within this range.

Figure 2 shows the voltammograms at two different illumination powers, 2 mW (red curve) and 10 mW (black curve), illustrating the strong dependence of the etch current on photo excitation. The blue trace in the main portion of Figure 2 shows that, if the light is turned off after PEC etching for some time, the etching current drops precipitously (red arrow), but that a small reduction current peak appears at ~ -0.1 V. This dip we attribute to re-deposition of In from In^{3+} generated during PEC etching.

3.3. Initial PEC etching kinetics: dependence on laser wavelength and intensity

In the presence of photoexcitation, in the initial stages of PEC etching of the InGaN thin film, an anodic current appears at ~ 0.1 V. As seen in Figure 3, this current increases with increasing laser intensity and decreasing laser wavelength, consistent with a photoexcited process and with an InGaN absorption coefficient that increases with increasing photon energy above its bandgap. Indeed, the sensitivity to wavelength is very strong, with the axes scales in Figures 3a, 3b and 3c decreasing by two orders of magnitude as wavelength increases from 420 to 430 to 440 nm. Negligible photocurrent was observed at laser wavelength longer than 450 nm, which is below the InGaN absorption band edge shown in Figure 1.

As shown in Figure 3, the magnitudes of the anodic currents and the shapes of the current-potential voltammograms over the studied voltage range depend on photo-excitation rate. At lower photo-excitation rates, due to either lower laser intensities or reduced absorption at longer laser wavelengths, the voltammograms are S-shaped: increasing rapidly at voltages just beyond 0.1 V, then saturating at voltages significantly beyond 0.1 V. At low voltages, surface oxidation is slow and rate-limiting. As voltage is increased, the rate of surface oxidation increases exponentially until ultimately becoming rate-limited by the photoexcitation, resulting in the observed S shapes.

At higher photo-excitation rates, due either to higher laser intensities or to increased absorption at shorter laser wavelength, the voltammograms (PEC etch rates) increase super linearly with voltage. However, *up to the maximum voltage examined* the PEC etch rates do not saturate, i.e., the S shape is not observed. The influence of mass transport due to laser heating is not discussed here since the variation in temperature at such low power intensities is negligible [20].

Figure 4 plots the PEC etch rate at 0.9 V versus photo-excitation rate at log scales. The photo-excitation rate has been calculated as the product, A**I*, of the laser intensity *I* and the light absorption coefficient measured from Figure 1. Once translated in this way into such a "unified" photo-excitation rate, one sees that the data points over the range of laser intensities studied and for the three excitation wavelengths appear to have a common slope close to 1, slightly decreasing from 0.93 at 420 nm to 0.86 at 440 nm. The etch efficiency, i.e., the ratio of the holes annihilated by etching versus absorbed photons, also decreases from 10 to 1% for the three wavelengths. It is decreased at the increase of the laser intensity. The detailed mechanistic interpretation of the different behaviors observed at different wavelengths is still under investigation. One possibility is that the excess absorbed energy above the band gap thermalizes within the lattice and contributes to the observed higher etching rates at shorter wavelength.

3.4. PEC etching dynamics: changes in kinetics over time

Thus far, we have discussed the kinetics during the initial stages of PEC etching of the InGaN thin film. As the process proceeds, the etching reaction rate evolves, as illustrated in Figures 5 and 6.

Figure 5 shows the etching dynamics during consecutive potential cycling where on each cycle the electrode potential was cycled up to the point just below the onset of the dark current associated with water oxidation. For the first 10 cycles, the voltammograms are nearly identical, and show a superlinear dependence of current on potential. On subsequent cycles, the voltammograms change shape: the PEC etching current increases at lower oxidation potentials and decreases at higher oxidation potentials (see traces #1, #12, and #16). After many cycles, the voltammograms becomes S-shaped, with the amplitude of the current at higher oxidation potentials continuing to decrease with continued cycling, initially rapidly and then more slowly.

We attribute these changes largely to a decrease in volume as the film etches and thus to a decrease in the total photo-excitation rate (per unit area illuminated and through the thickness of

the film). However, we note that as the film is etching, its morphology is also changing: first roughening and then ultimately evolving into very small, ~ 2 to 5 nm scale nanoparticles (see Figure 7, discussed below). These nanoparticles are in the quantum size regime, leading to increased bandgaps when their diameters are further decreased.

How this roughening and eventual nanoparticle formation influences the PEC etch currents is illustrated in Figure 6, which plots the PEC etch current as a function of time at a constant potential of 0.9 V and for various starting film thicknesses. After an initial current transient due to non-Faradaic double-layer charging, for each laser intensity (Figure 6a) and film thickness (Figure 6b) the PEC etch current follows a characteristic pattern: first, an incubation period; second, a rise to a peak etch rate; and, third, a decay with a long tail.

Our proposed interpretation for this pattern is the following. The initial incubation period is due to two offsetting phenomena: as the film etches the total absorption rate through the film thickness (and, thus, carrier creation rate) decreases, causing the etch rate to decrease; but as the film roughens, surface area increases, causing the etch rate to increase. Eventually the surface area effect becomes stronger and the etch rate increases until it reaches a peak at which the product of light absorption and surface area is maximum. Subsequently, surface area no longer increases but film volume continues to decrease, leading to the observed etch rate decrease. In addition, as the nanoparticles that are formed enter the quantum size regime, the bandgap of these nanoparticles increase, leading to an even more pronounced drop in light absorption and etch rate.

This interpretation is consistent with a longer incubation time at lower laser intensities, assuming the morphology evolution is similar but just slower. It is also consistent with an incubation time that decreases with decreasing film thickness, since this would require a shorter time for the surface roughness to reach a peak (Figure 6b). Quantum dots (quantum sized nanoparticles) are also made quicker from thinner films.

3.5. Surface nanostructuring from InGaN thin films

All of the etch curves show a current decay with a very long tail. This highlights a unique characteristic of semiconductor etching promoted by photoexcitation, unlike any other chemical or electrochemical etching that continues until the etched material is completely removed, such as in metal striping. In the PEC etch process discussed here a high density of nanoparticles are formed.

Figure 7 shows AFM images of the evolving surface. The initial film (Figure 7a, inset) is atomically smooth with visible step/terrace structures. Spiral growth with pin holes is seen across most of the surface. The steps are mostly monoatomic, the terraces are often less than 100 nm in width, and the surface is rich in kinks and intersecting steps. After 100 consecutive potential cycles of etching (shown as in Figure 5), nanoparticles of relatively uniform size are formed on the surface. The height of the nanoparticles is around 2 to 3 nm (figure 7b, c).

As illustrated in Figure 8, we have also PEC etched a very different initial structure composed of an array of InGaN/GaN nanowires. These nanowires were fabricated using a top-down lithographic method, and contained 3-nm-thick InGaN quantum wells separated by 10 nm GaN layers [21]. The rest of the nanowires at both ends are thicker GaN layers, so PEC etching at wavelengths below the GaN bandgap can occur only laterally from the edges (Figure 8a inset, and Figure 8b). For these structures, because there is no film roughening, but instead the InGaN disks within the nanowires simply etch radially inwards, there is no incubation time. Instead, the current decreases exponentially with time as volume and associated photoexcitation rate decrease.

After lateral etching for 5 minutes, these quantum wells were etched laterally inwards by about 2 nm. However, the GaN barrier layers were also partially etched. The bottom faces of the quantum wells were etched deeper than the top portions, forming a horizontally asymmetric V-shape. Because the MOVPE-grown material is oriented with the N-face down, this image provides *atomic resolution* evidence of the preferential PEC etching of N-faces over the Ga-faces [15, 22]. After 15 minutes, the lateral etch-distance increases to ~ 30 to 40 nm (Figure 8d). Again, most of the GaN layers were affected at the N-faces, while the top Ga-faces remained unetched. Because these nanowires were etched at 405 nm laser wavelength, which is close to the absorption band edge of GaN, the bandgap selection alone is insufficient to etch selectively etch only the InGaN.

4. Conclusions

Photoelectrochemical etching methods can be controlled to significantly enhance the etch rate of III-N materials, that is dependent on the laser wavelength, laser power intensity, and electrochemical potential. Depending on the laser wavelength, the observed etch rate ranged from superlinear to S shape with the applied electrode potentials during initial etching of the films. After some degree of etch, all etch curves were found to exhibit the S shape upon nanoparticle formation. As the etching proceeds to long times, the remaining InGaN material texture became

nanostructured with nanoparticles approaching the quantum size limit. Because the decrease of the particle size results in the decrease of light absorption, due to the decreased volume of film for light absorption and to the increase of the bandgaps of the resulting nanoparticles due to quantum confinement effects, in principle, a self-limited etch kinetics would be established.

Acknowledgements

Work at Sandia National Laboratories was supported by Sandia's Solid-State Lighting Science Energy Frontier Research Center, funded by the U.S. Department of Energy, Office of Basic Energy Science. The work was also partially funded by Sandia's LDRD program. Sandia National Laboratories is a multi-program laboratory managed and operated by Sandia Corporation, a wholly owned subsidiary of Lockheed Martin Corporation, for the U.S. Department of Energy's National Nuclear Security Administration under contract DE-AC04-94AL85000. We thank S. Casalnuovo, E. Spoerke, G. Montano, I. Brener, and R.P. Schneider for helpful discussions.

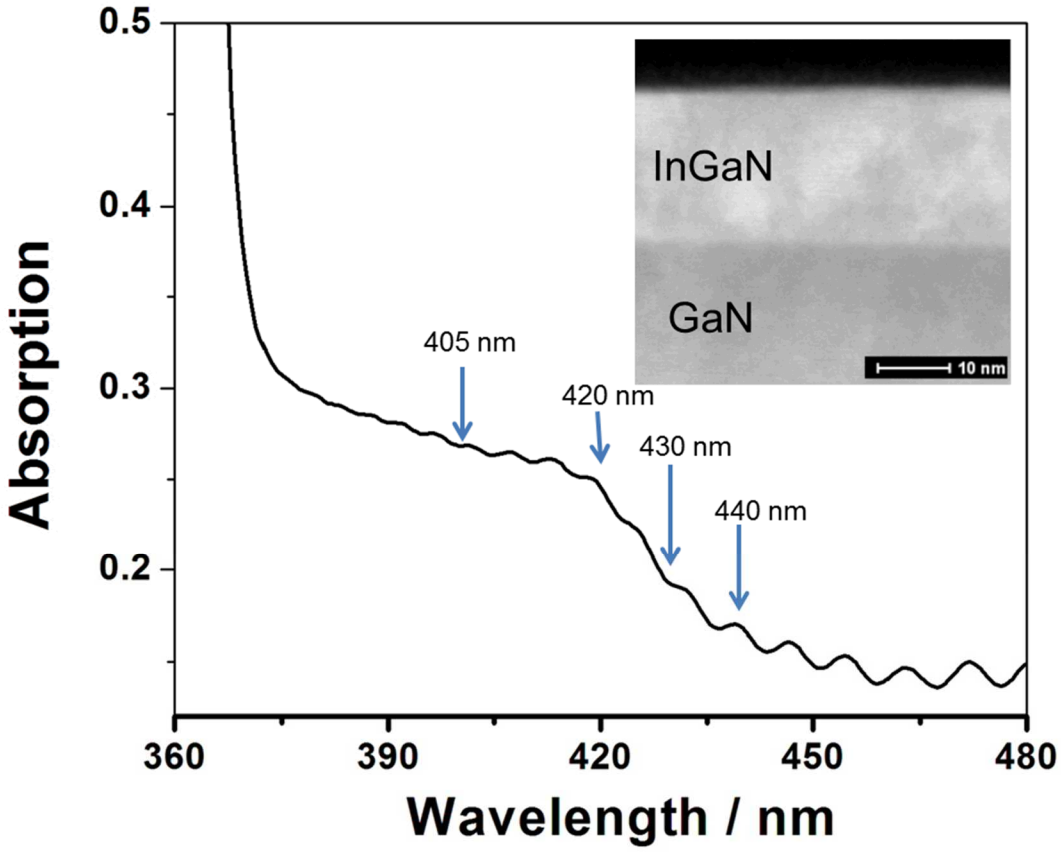

Figure 1. Optical absorption spectrum of a 20-nm-thick $In_{0.13}Ga_{0.87}N$ epitaxial film on a 5-μm-thick GaN buffer layer on a sapphire substrate. Insert, cross-section STEM image of the film. The arrows indicate the wavelengths of the lasers used for PEC etching in this paper.

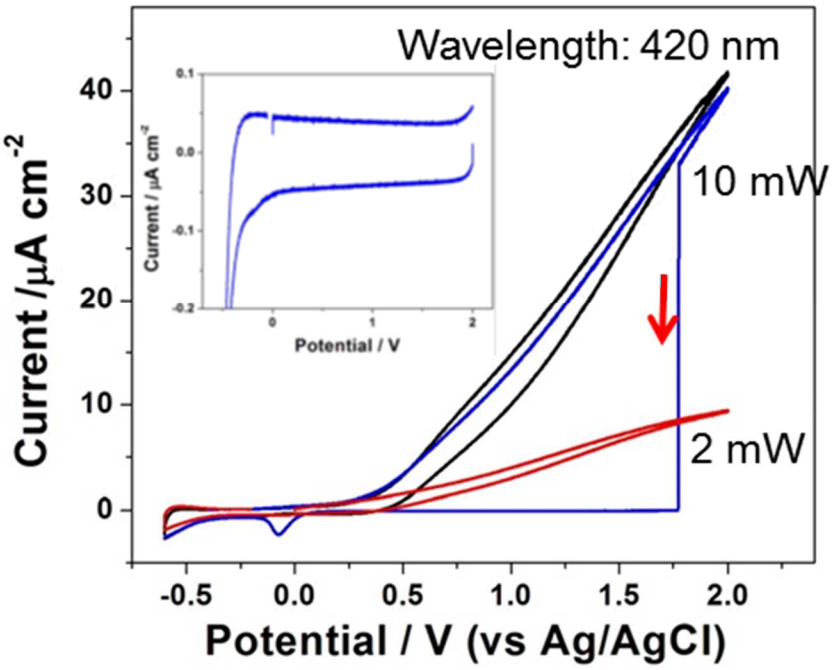

Figure 2. The dependence of PEC etch dynamics on laser power intensity at 420 nm laser excitation. 10 nm InGaN epi-film, 0.2 M H_2SO_4, 0.2 V/s. The laser intensity is indicated in the figures. The red arrow indicates the laser being blocked. The inset was the voltammogram recorded in the dark.

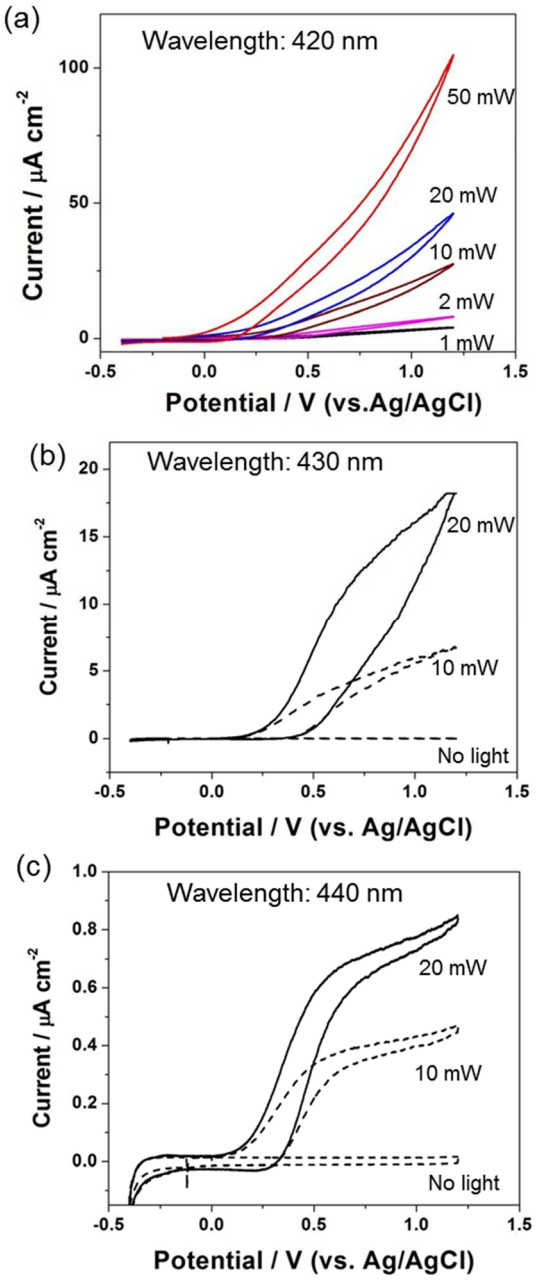

Figure 3. The dependence of PEC etch dynamics on laser wavelength and power intensity. 10 nm InGaN epi-film, 0.2 M H_2SO_4, 0.2 V/s. The laser wavelength and intensity are indicated in the figures, respectively.

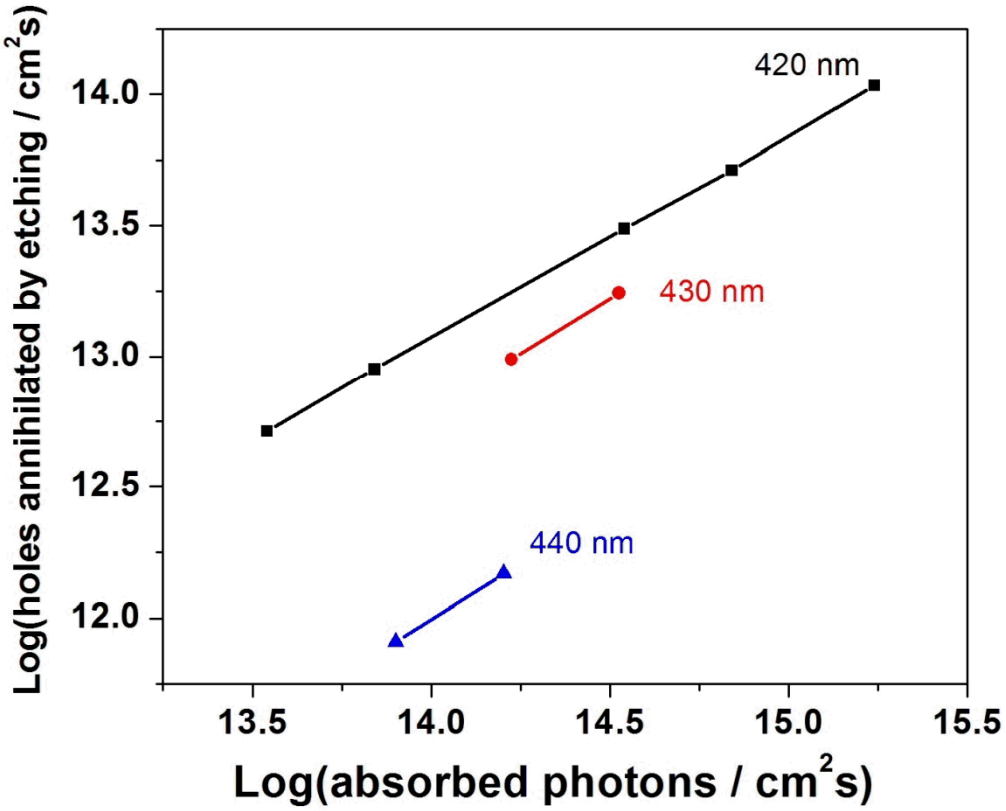

Figure 4. The dependence of PEC etch rate at 0.9 V on photo-excitation rate at Log scales from a 10 nm InGaN film.

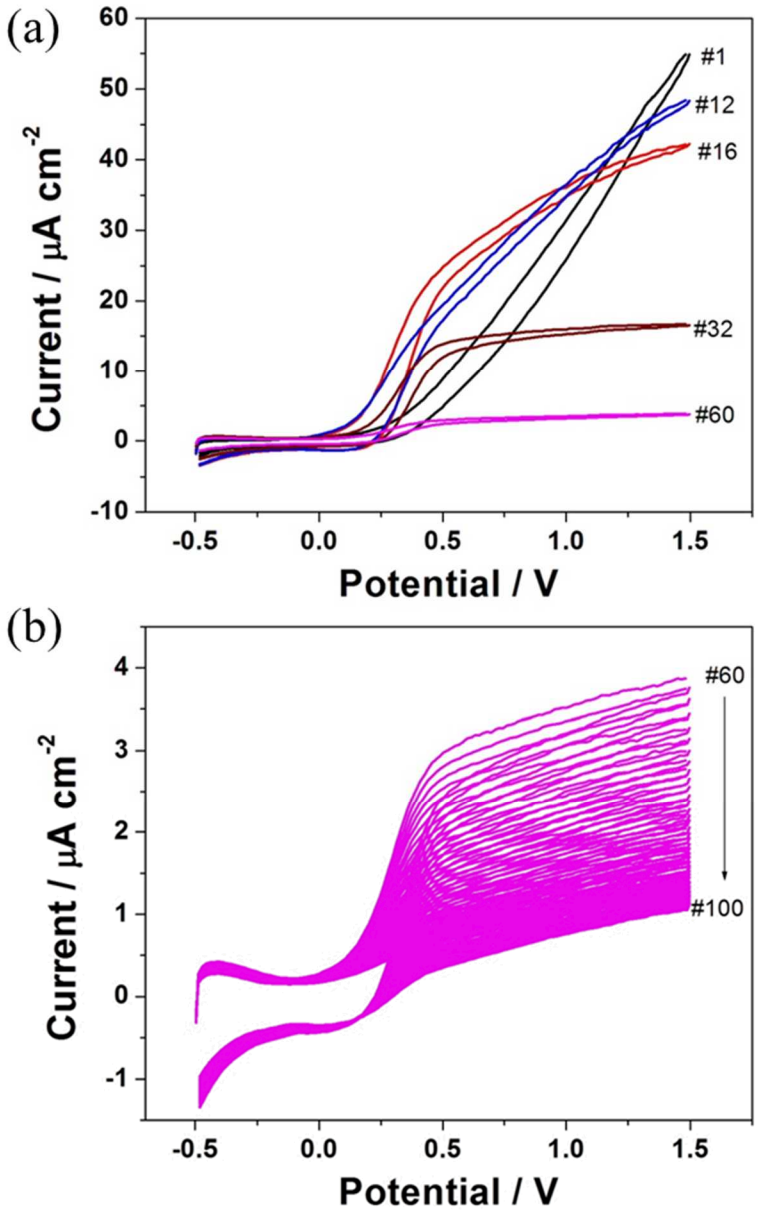

Figure 5. Etch dynamics during consecutive potential cycling of a 10 nm InGaN epi-film in 0.2 M H_2SO_4 at 0.2 V/s. The number of potential cycles with corresponding features was indicated. The laser: 420 nm, ~ 10 mW.

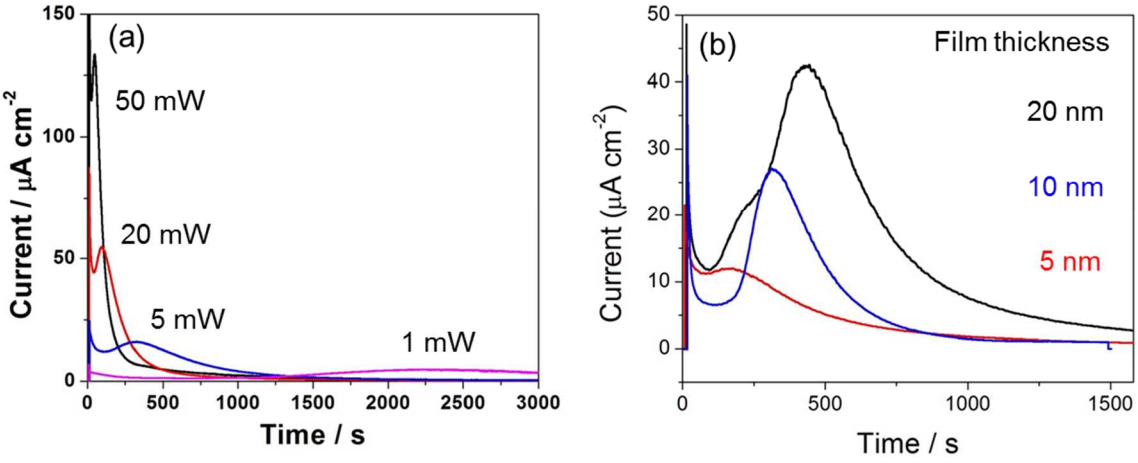

Figure 6. PEC etching current evolution at a constant potential of 0.9 V. (a) 10 nm film, variable laser intensity. (b) 5 mW laser intensity, variable film thickness. Electrolyte: 0.2 M H_2SO_4. The laser wavelength was 420 nm.

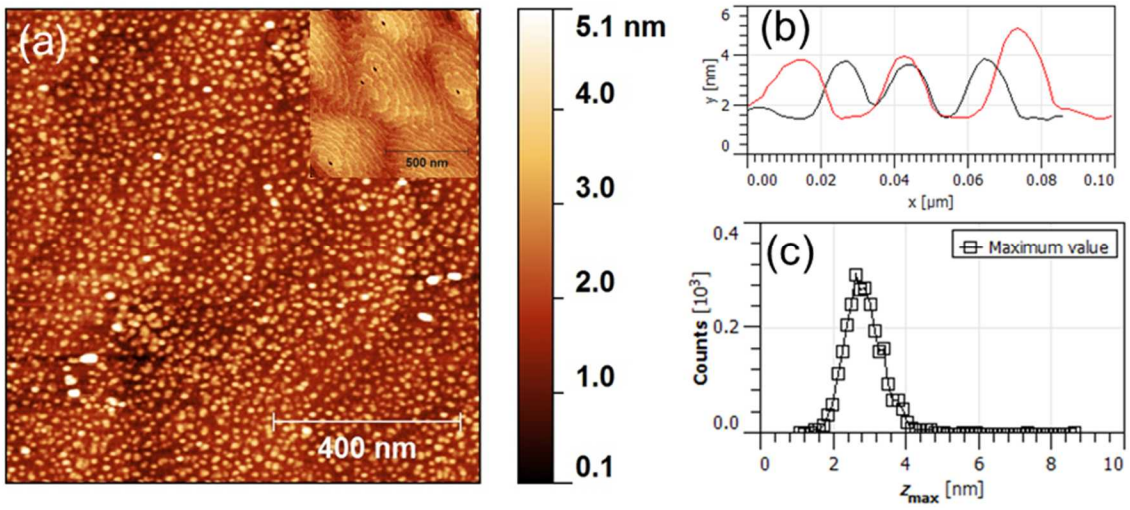

Figure 7. AFM analysis of InGaN nanoparticles formed after PEC etching of a 10 nm film by 100 potential cycles. (b) Cross-section profiles of dots across two sections of the etched film, (c) dot height distribution across the AFM image. The potential cycling was described as in Figure 5. The inset is a typical AFM image of the film before PEC etching.

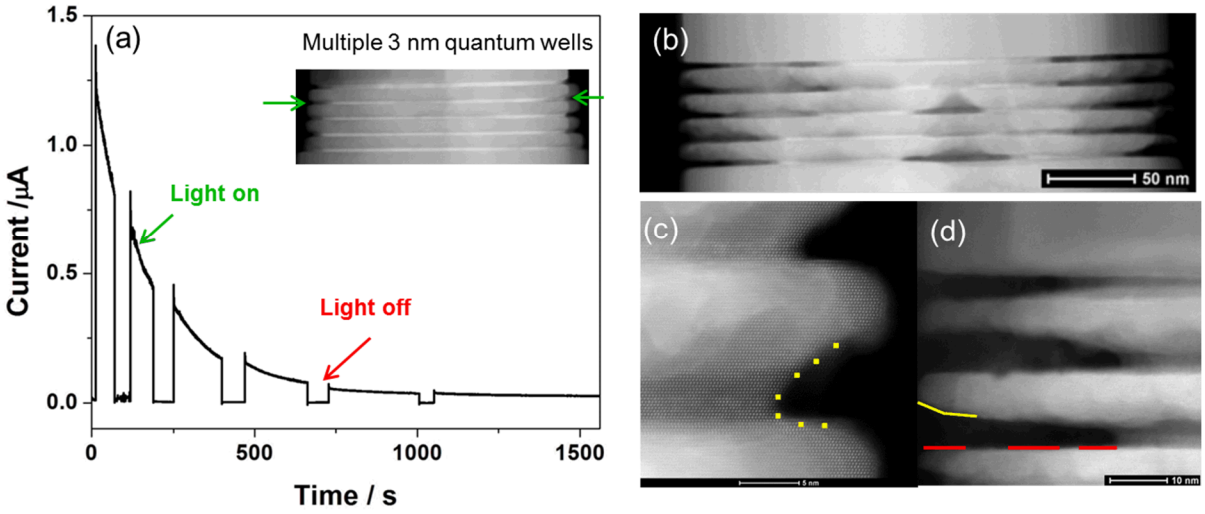

Figure 8. PEC etch dynamics of an InGaN/GaN nanowire consisting of multiple 3-nm-thick InGaN quantum wells embedded in GaN. (a) light-controlled current dynamics, (b) STEM image after etch for 900 s at 0.9 V, (c, d) high resolution STEM images after 300 and 900 s etch, respectively.

References

1. Ponce, F.A. and D.P. Bour, *NItride-based semiconductors for blue and green light-emitting devices.* Nature, 1997. **386**(6623): p. 351-359.
2. Arakawa, Y., *Progress in GaN-based quantum dots for optoelectronics applications.* Ieee Journal of Selected Topics in Quantum Electronics, 2002. **8**(4): p. 823-832.
3. Saito, T. and Y. Arakawa, *Electronic structure of piezoelectric In0.2Ga0.8N quantum dots in GaN calculated using a tight-binding method.* Physica E-Low-Dimensional Systems & Nanostructures, 2002. **15**(3): p. 169-181.
4. Mohammad, S.N., A.A. Salvador, and H. Morkoc, *Emerging Gallium Nitride Based Devices.* Proceedings of the Ieee, 1995. **83**(10): p. 1306-1355.
5. Khan, M.A., et al., *GaN based heterostructure for high power devices.* Solid-State Electronics, 1997. **41**(10): p. 1555-1559.
6. Pearton, S.J. and F. Ren, *GaN electronics.* Advanced Materials, 2000. **12**(21): p. 1571-+.
7. Jung, Y., et al., *Chemical Etch Characteristics of N-Face and Ga-Face GaN by Phosphoric Acid and Potassium Hydroxide Solutions.* Journal of the Electrochemical Society, 2012. **159**(2): p. H117-H120.
8. Adesida, I., et al., *Dry and wet etching for group III-nitrides.* Mrs Internet Journal of Nitride Semiconductor Research, 1999. **4**.
9. Huygens, I.M., K. Strubbe, and W.P. Gomes, *Electrochemistry and photoetching of n-GaN.* Journal of the Electrochemical Society, 2000. **147**(5): p. 1797-1802.
10. Karouta, F., et al., *High etch rate and smooth morphology using a novel chemistry in reactive ion etching of GaN.* Electrochemical and Solid State Letters, 1999. **2**(5): p. 240-241.
11. Vartuli, C.B., et al., *Wet chemical etching of AlN and InAlN in KOH solutions.* Journal of the Electrochemical Society, 1996. **143**(11): p. 3681-3684.
12. Vartuli, C.B., et al., *Selective dry etching of III-V nitrides in Cl-2/Ar, CH4/H-2/Ar, ICI/Ar, and IBr/Ar.* Journal of the Electrochemical Society, 1996. **143**(10): p. L246-L248.
13. Vartuli, C.B., et al., *High density plasma etching of III-V nitrides.* Journal of Vacuum Science & Technology a-Vacuum Surfaces and Films, 1996. **14**(3): p. 1011-1014.
14. Peng, L.H., et al., *Deep ultraviolet enhanced wet chemical etching of gallium nitride.* Applied Physics Letters, 1998. **72**(8): p. 939-941.
15. Gao, Y., et al., *Dislocation- and crystallographic-dependent photoelectrochemical wet etching of gallium nitride.* Applied Physics Letters, 2004. **84**(17): p. 3322-3324.
16. Youtsey, C., G. Bulman, and I. Adesida, *Dopant-selective photoenhanced wet etching of GaN.* Journal of Electronic Materials, 1998. **27**(4): p. 282-287.
17. Jung, Y., et al., *Effects of Photoelectrochemical Etching of N-Polar and Ga-Polar Gallium Nitride on Sapphire Substrates.* Journal of the Electrochemical Society, 2010. **157**(6): p. H676-H678.
18. Huygens, I.M., et al., *Photoelectrochemical reactions at the n-GaN electrode in 1 M H2SO4 and in acidic solutions containing Cl- ions.* Physical Chemistry Chemical Physics, 2002. **4**(11): p. 2301-2306.
19. Xiao, X., et al., *in preparation*.
20. Lax, M., *Temperature Rise Induced by a Laser-Beam.* Journal of Applied Physics, 1977. **48**(9): p. 3919-3924.

21. Wang, G.T., et al., *Highly aligned, template-free growth and characterization of vertical GaN nanowires on sapphire by metal-organic chemical vapour deposition.* Nanotechnology, 2006. **17**(23): p. 5773-5780.
22. Bae, H., et al., *The Polarity Effect on the Photoelectrochemical Properties of Ga- and N-Face Free-Standing GaN Substrate.* Japanese Journal of Applied Physics, 2013. **52**(8).